Artificial p–n-like Junction Based on Pure 2D Organic–Inorganic Halide Perovskite Structure Having Naphthalene Diimide Acceptor Moieties

Zhao Feng, Xuelong Liu, Kentaro Imaoka, Tomohiro Ishii, Ganbaatar Tumen-Ulzii, Xun Tang, George Harrington, Benoît Heinrich, Jean-charles Ribierre, Lise-marie Chamoreau, et al.

Artificial p-n like junction based on naphthalene diimide acceptor moieties confined in pure 2D organic-inorganic halide perovskite structure

Zhao Feng[1,6], Tomohiro Ishii[1], Ganbaatar Tumen-Ulzii[1,2], Xuelong Liu[1], Xun Tang[1], George F. Harrington[2], Benoit Heinrich[3], Jean-Charles Ribierre[1], Lise-Marie Chamoreau[4], Lydia Sosa Vargas[4], David Kreher[4,5], Kenichi Goushi[1], Toshinori Matsushima[2], Guijiang Zhou[6], Fabrice Mathevet[1,4*], Chihaya. Adachi[1,2*]*

1. Center for Organic Photonics and Electronics Research (OPERA) and Department of Applied Chemistry, Kyushu University, 744 Motooka, Nishi, Fukuoka 819-0395, Japan.
2. International Institute for Carbon Neutral Energy Research (WPI-I2CNER), Kyushu University, 744 Motooka, Nishi, Fukuoka 819-0395, Japan.
3. Institut de Physique et Chimie des Matériaux de Strasbourg (IPCMS), UMR 7504, CNRS-Université de Strasbourg, 23 Rue du Loess, 67034 Strasbourg Cedex 2, France.
4. Sorbonne Université, CNRS, Institut Parisien de Chimie Moléculaire (IPCM), UMR 8232, F-75005 Paris, France.
5. Institut Lavoisier de Versailles (ILV), UMR-CNRS 8180, Université de Versailles-Saint-Quentin-en-Yvelines, 45 avenue des Etats-Unis, 78035 Versailles cedex, France.
6. School of Chemistry, MOE Key Laboratory for Nonequilibrium Synthesis and Modulation of Condensed Matter, Xi'an Key Laboratory of Sustainable Energy Material Chemistry, Xi'an Jiaotong University, Xi'an 710049, P. R. China.

Correspondence and requests for materials should be addressed to GZ, FM or C.A. (email: zhougj@xjtu.edu.cn, fabrice.mathevet@sorbonne-universite.fr; adachi@cstf.kyushu-u.ac.jp)

Keywords: 2D perovskite, naphthalene diimide (NDI), p-n heterojunction, electron transfer, charge separation, photoconduction.

Abstract

Two-dimensional (2D) organic-inorganic perovskites are an emerging class of materials with a great potential since a wide variety of large functional chromophores can be regularly incorporated. Among this new type of materials, hybrid perovskite systems incorporating strong electron acceptor molecules are considered as a promising approach to design a new type of functional 2D perovskites for optoelectronics. In this work, a rare example of organic-inorganic 2D perovskite incorporating strong acceptors such as naphthalene diimide (NDI) building blocks between inorganic sheets is presented. This hybrid architecture is easily obtained via a solution deposition process to form highly air-stable thin films with a structure consisting of inorganic perovskite monolayers of metal-halide octahedra separated by bi-layers of NDI-based organic cations. The presence of strong electron-accepting moieties in this multifunctional donor-acceptor hybrid heterostructure led to a scarce type II heterojunction in which the excitons can be efficiently dissociated via the electron transfer process and in which holes and electrons can be easily confined in the inorganic and organic sublayer, respectively. Such an ultimate p-n heterojunction showed improved photoconduction properties with a photocurrent multiplied by 40 under white-light illumination in comparison to a similar 2D perovskite structure containing simply inert alkyl chains as organic components.

Introduction

Two-dimensional (2D) organic-inorganic perovskites are an emerging class of materials with a great potential since a wide variety of functional chromophores can be regularly incorporated, resulting in elaborate electronic or optoelectronic devices such as light-emitting diodes (LEDs), solid-state lasers, field-effect transistors (FETs), solar cells, and photodetectors.[1–4] 2D hybrid perovskites differ from their tri-dimensional (3D) counterparts by the presence of large organic cations that lead to a layered structure consisting of 2D inorganic metal-halide octahedra layers separated by organic cations. Generally, these organic cations incorporated in 2D perovskites are simple alkyl- or phenyl alkyl-ammonium salts and, except for their effect on the inorganic sheets separation, they do not contribute any specific functionality or optoelectronic properties to the system.[5–10]

Recently 2D perovskites incorporating more complex organic cations have been widely investigated. For instance, in the pioneering works of Mitzi et al., 2D perovskites based on quaterthiophene diammonium cations were successfully prepared. In this work, the authors investigated the structure-property relationships of such a hybrid material and examined the photoluminescence (PL) and electroluminescence (EL) properties of the organic part.[11,12] Recently, several new functional organic cations such as large electron-rich aromatic molecules,[13–15] donor-acceptor π-conjugated systems[14,16] and charge transfer complexes[17] have also been incorporated into 2D perovskites. These hybrid materials showed promising properties such as an enhanced out-of-plane conductivity by tunneling through the organic layers[13] and the controllability of either organic or inorganic layers' PL by the fine-tuning of the organic cation's energy levels.[14]

Hybrid perovskite systems incorporating strong electron acceptor molecules are also considered as a promising approach to design a new type of "functional" 2D perovskites. In such structures, the

bandgaps for the inorganic and organic layers can be offset, leading to a hybrid donor-acceptor heterostructure, i.e., type II quantum well system, in which the wells for the holes and electrons are located in different layers.[18–20] This configuration is particularly interesting because it can lead to strongly enhanced charge separation and the formation of long-lived mobile charge carriers useful for optoelectronic devices. For instance, a few examples of hybrid perovskite structures incorporating perylene (PDI)[21] or naphthalene (NDI)[22–24] diimide derivatives as acceptor units have been reported, providing efficient charge carrier separation and ambipolar conduction. However, all these hybrid heterostructures were designed based on quasi 2D perovskite systems as inorganic layers and almost no "pure" 2D perovskite incorporating PDI or NDI strong acceptors has been synthesized and investigated yet, except the very recent report by S. Nussbaum *et al*..[25]

Herein, we report a stable 2D perovskite structure **(monoNDIC8)$_2$PbI$_4$** consisting of inorganic monolayers of metal-halide octahedra separated by bi-layers of NDI-based monoammonium organic cations **monoNDIC8**. We investigated the thin film structure and morphology of this organic-inorganic architecture, as well as its crystal structure. We also explored the impact of the strong electron-accepting NDI moieties in the donor-acceptor hybrid heterostructure **(monoNDIC8)$_2$PbI$_4$** on its electronic, photophysical and charge separation properties in comparison with that of a "more conventional" non-functional 2D perovskites **(C8)$_2$PbI$_4$**, incorporating simple alkylammonium salts as the organic cation. Finally, we investigated the photoconductivity properties of this D-A hybrid material in device configuration to clarify its potential for optoelectronic applications.

Results and discussion

Synthesis and characterizations. To prepare the 2D perovskites, **(monoNDIC8)$_2$PbI$_4$** and **(C8)$_2$PbI$_4$**, we designed and synthesized, as a first step, the two organic cations of **monoNDIC8** and **C8** (see the chemical structures in Figure 1a). The detailed synthetic procedures for the target organic cations are given in the supporting information section. The 2D perovskite thin films of **(monoNDIC8)$_2$PbI$_4$** and **(C8)$_2$PbI$_4$** were prepared by a typical one-step spin-coating method from precursor solutions with a ratio between the ammonium salt and PbI_2 of 2:1 (see experimental methods). UV-vis absorption and PL spectra of the two thin films were firstly measured to confirm the 2D perovskite formation. Both **(monoNDIC8)$_2$PbI$_4$** and **(C8)$_2$PbI$_4$** absorption spectra showed sharp excitonic absorption peaks located at 500 nm and 511nm, respectively, which are associated with the bandgap of the inorganic frameworks and are characteristic for pure 2D layered lead iodide perovskites.[11,18,26] In addition to the excitonic peak, the absorption spectrum of **(monoNDIC8)$_2$PbI$_4$,** shows an intense structured band between 300 nm and 400 nm which corresponds to the absorption of the NDI cores confined inside the organic sublayers as evidenced in Figure S1a.

The PL spectra of **(monoNDIC8)$_2$PbI$_4$** and **(C8)$_2$PbI$_4$** thin films present sharp emission peaks (with a full width at half maximum of 20 nm) located at 511 nm and 521 nm, respectively, indicating that the PL spectra originates from inorganic perovskite sublayers (Figure 1c).[14,18] However, the observed PL for a **(monoNDIC8)$_2$PbI$_4$** thin film is significantly quenched compared to that of a **(C8)$_2$PbI$_4$** thin film. This observation suggests a possible photoinduced charge transfer between the perovskite monolayers and the NDI components leads to charge separation, as already observed in quasi-2D and 2D perovskites[23,24,25] based on NDI salts, and perovskite nanoplatelets surrounded by PDIs.[21] To investigate the effect of the NDI cores confined in the 2D perovskite structure on the exciton lifetimes,

we performed picosecond time-resolved PL measurements using a streak camera (Figures 2a and 2b). Here, we compared the PL decays of **(monoNDIC8)$_2$PbI$_4$** and **(C8)$_2$PbI$_4$** to clarify the effect of alkyl-NDI and simple alky chain sublayers (Figure 2c). Noticeably, the PL lifetime of the **(monoNDIC8)$_2$PbI$_4$** perovskite structure (~ 30 ps) is significantly reduced compared to that of **(C8)$_2$PbI$_4$** (~ 200 ps), suggesting the presence of a rapid electron transfer to the electron-accepting NDIs from the excitons in the inorganic sheets. It is also interesting to note that a small residual emission of the NDI cores can be observed for the **(monoNDIC8)$_2$PbI$_4$** thin film (Figure S1b), indicating that the charge separation between the organic and inorganic sublayers is not complete, which is probably due to the presence of the long alkyl spacer separating the perovskite monolayers and the NDI units.

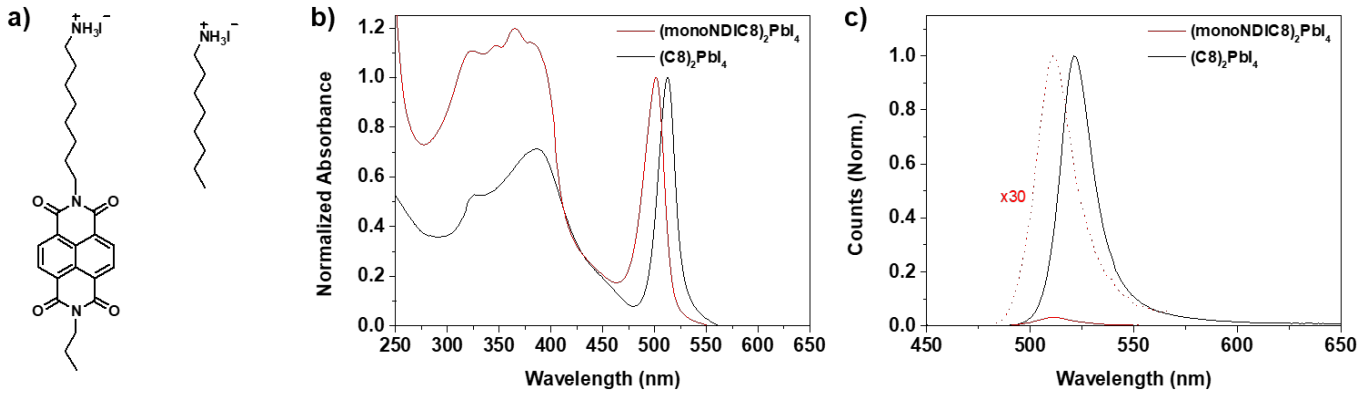

Figure 1. a) Chemical structures of the **monoNDIC8** and **C8** organic cations. b) Normalized UV-vis absorption and c) PL spectra of **(monoNDIC8)$_2$PbI$_4$** and **(C8)$_2$PbI$_4$** perovskite thin films (For emission spectra in solid line, λ_{ex} = 390 nm with a normalized O.D.).

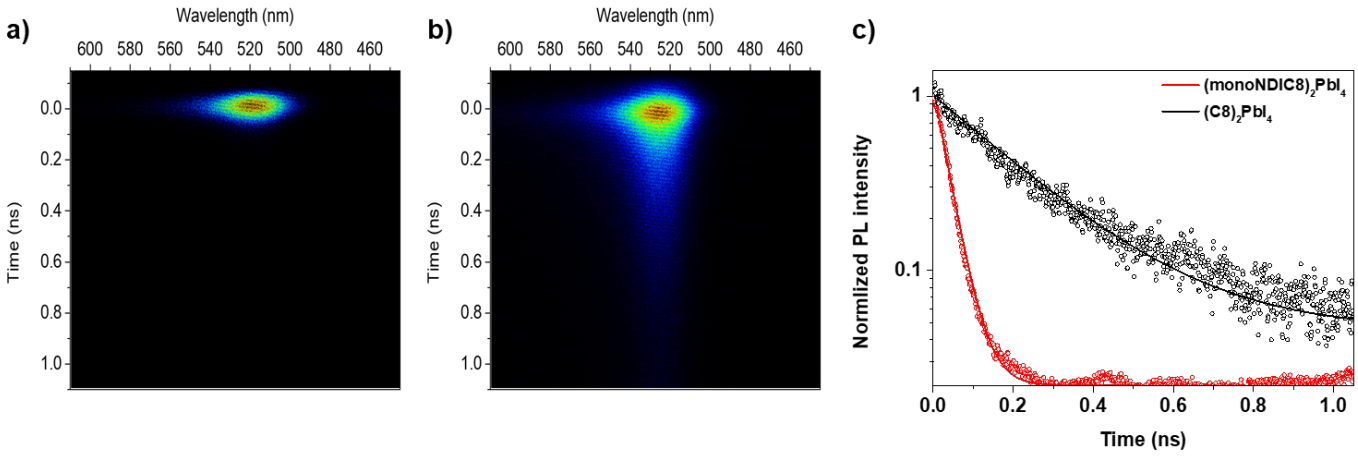

Figure 2. Photoluminescence of a) **monoNDIC8** and b) **$(C8)_2PbI_4$** thin films as a function of time and wavelength. c) Comparison of the PL temporal decay of **monoNDIC8** and **$(C8)_2PbI_4$** thin films showing the fluorescence quenching that could be explained by electron transfer to NDI units.

The thin film structures of **$(monoNDIC8)_2PbI_4$** and **$(C8)_2PbI_4$** perovskites were then investigated by X-ray diffraction (XRD). Their out-of-plane and in-plane XRD patterns are shown in (Figures 3a and 3b). Both out-of-plane patterns show a series of intense, sharp and equidistant reflections corresponding to the (*h*00) spacing of the 2D layered perovskite structure and indicating a long-range lamellar order with high crystallinity (Figures 3a and 3b, bottom). In addition, for both **$(monoNDIC8)_2PbI_4$** and **$(C8)_2PbI_4$** thin films, no lamellar reflections are observed in the in-plane XRD patterns, suggesting a preferential orientation of the layered structure with the organic and inorganic perovskite sublayers parallel to the substrate (Figure 3a and 3b, top). Based on the lamellar reflections in the out-of-plane XRD patterns of both **$(monoNDIC8)_2PbI_4$** and **$(C8)_2PbI_4$** thin films, the interlayer spacings (*d*) between the inorganic perovskite sublayers were calculated to be 38.6 Å and 18.7 Å, respectively. We note that the *d*-spacing value of 18.7 Å obtained for the **$(C8)_2PbI_4$** thin

film is in good agreement with the value reported in the literature (d = 18.6 Å) and extracted from the crystal structure of **(C8)$_2$PbI$_4$** (see Figure S2).[7] Regarding the d-spacing observed in the **(monoNDIC8)$_2$PbI$_4$** thin film (d = 38.6 Å), such a large value suggests a probable bilayer organization of the organic cations **monoNDIC8** that is consistent with the larger cross-section of the NDI cores than that of the simple alkyl chains, precluding their interdigitation.

To further investigate the structure of **(monoNDIC8)$_2$PbI$_4$**, bulk crystals were prepared by antisolvent vapor diffusion method from a precursor solution (see supporting information) and the obtained single crystals were resolved using single crystal X-ray diffraction. The side view of the layered organization of a **(monoNDIC8)$_2$PbX$_4$** crystal is displayed along the b-axis in Figure 3c, left (for more structure details, see Supporting Information and Table S1). The crystal structure clearly confirms the bilayer organization of the **monoNDIC8** salts between the halide perovskite monolayers and shows an interlayer spacing of around 41 Å which is consistent with the large value previously observed for **(monoNDIC8)$_2$PbI$_4$** thin films. The crystal structure also evidences the herringbone packing of the NDI cores in the plane of the NDI sublayers (Figure 3d, right) which is known to be a favorable 2D molecular packing arrangement for efficient layered charge transport.[27,28]

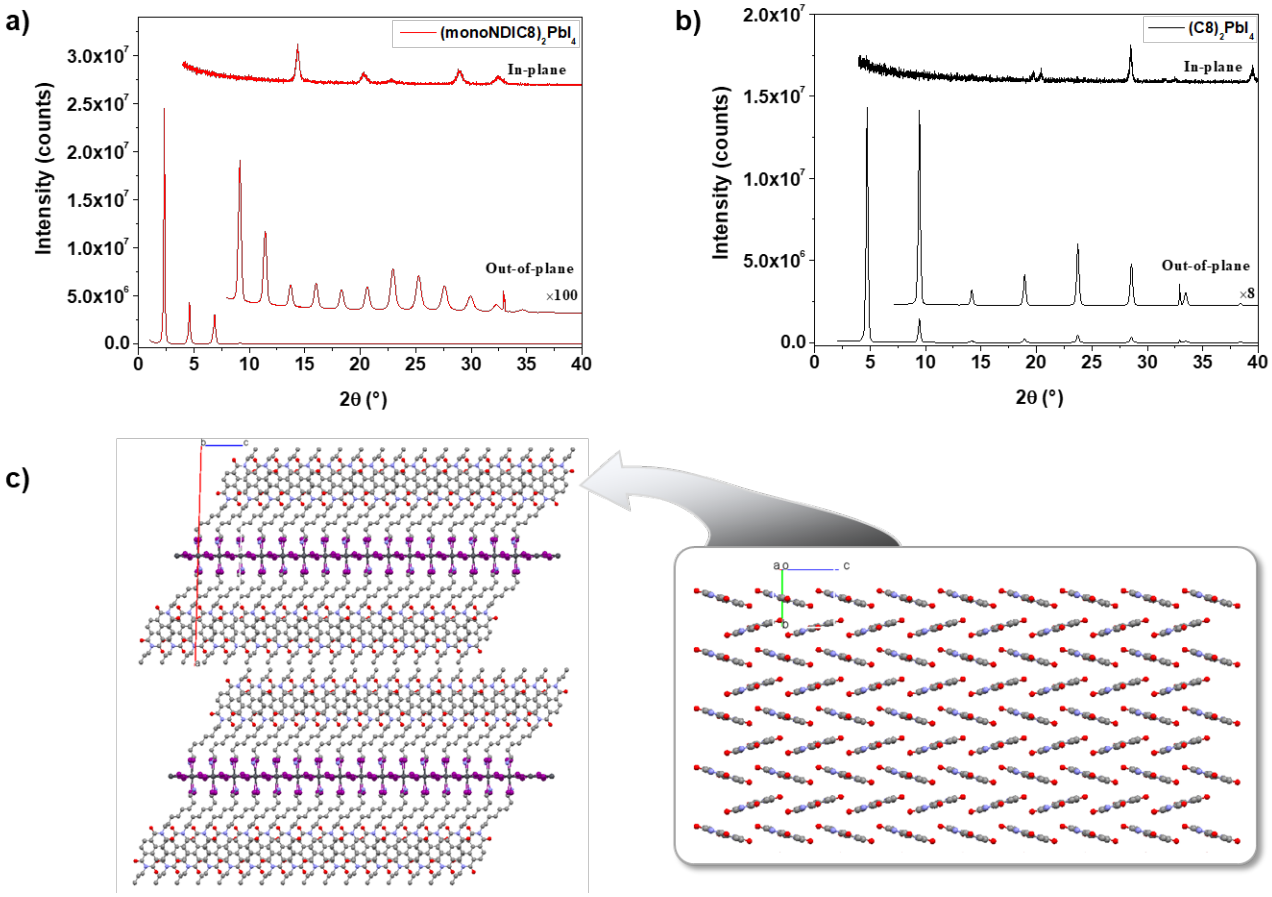

Figure 3. X-ray patterns of a) **(monoNDIC8)$_2$PbI$_4$** and b) **(C8)$_2$PbI$_4$** perovskite thin films. Bottom and top patterns correspond to out-of-plane and in-plane measurements, respectively. c) (Left) Representation of the monoclinic single crystal structure of the 2D perovskite **(monoNDIC8)$_2$PbX$_4$**, view along *b*-axis of the lamellar sequence showing the bilayer organization of NDIs between the halide perovskite monolayers. (Right) Representation of the herringbone arrangement of NDI aromatic cores inside an NDI sublayer. (Note that hydrogen atoms are removed for clarity)

The stability of the **(monoNDIC8)$_2$PbI$_4$** and **(C8)$_2$PbI$_4$** perovskite materials towards moisture was also considered in view of practical applications. To this end, the thin films of **(monoNDIC8)$_2$PbI$_4$** and **(C8)$_2$PbI$_4$** were continuously exposed to an ambient environment and their degradation was monitored by XRD. As a result, the **(C8)$_2$PbI$_4$** 2D perovskite shows poor stability towards ambient

conditions, as over 30% of the intensity of its original first-order diffraction peak was lost in the XRD patterns after only 4 h of exposure (Figure S4a). This degradation is consistent with the previous investigations performed on 2D halide perovskites based on mono-alkylammonium cations showing that oxygen and moisture can easily penetrate through the simple hydrophobic alkyl chain barrier layer due to the small size and weak intermolecular interaction of the aliphatic chains.[14] In contrast, the **(monoNDIC8)$_2$PbI$_4$** 2D perovskite shows better stability than the **(C8)$_2$PbI$_4$**, since no decrease of the first-order diffraction peak was observed in the XRD patterns after one week of exposure to air and a loss of only 5% after 60 days (Figure S4b). This improved stability is due to the incorporation of NDI units, which are bulky, hydrophobic, and can be seen as aggregated building blocks with strong intermolecular interactions that can effectively block the oxygen and moisture penetration into the inorganic perovskite sublayers. This promising result is consistent with the recent reports of 2D halide perovskites incorporating large π-conjugated organic ammonium cations, also showing an improved intrinsic stability.[14,20,29]

Since 2D organic-inorganic hybrid halide perovskites present a quantum-well structure, the determination of the highest occupied molecular orbital (HOMO) and lowest unoccupied molecular orbital (LUMO) alignments/offsets between the organic and inorganic perovskite sublayers is one of the key parameters for future optoelectronic applications. Thus, we investigated the band alignments in our two, 2D perovskite systems. To this end, we measured the HOMO and LUMO levels for **(C8)$_2$PbI$_4$** and **(monoNDIC8)$_2$PbI$_4$** perovskite thin films, as well as the **NDIC3** derivative (See SI for the chemical structure), by photoelectron spectroscopy (PES) and low-energy inverse photoemission spectroscopy (LEIPS). Theoretically, the HOMO and LUMO levels of **NDIC3** represent those of the organic sublayers in **(monoNDIC8)$_2$PbI$_4$**, since they share the same NDI core with just a small

difference in alkyl chain length. According to the PES data, the HOMO levels of **$(C8)_2PbI_4$**, **$(monoNDIC8)_2PbI_4$**, and **NDIC3** are -5.87, -5.80, and -6.42 eV, respectively (Figure S5). LEIPS measurements show that the LUMO levels of **$(monoNDIC8)_2PbI_4$** and **NDIC3** are -3.63 and -3.71 eV, respectively (Figure S6). Unfortunately, we could not detect the LUMO level of **$(C8)_2PbI_4$** by LEIPS due to its severe degradation under the electron beam exposure, and this later was approximated to be -3.49 eV from the UV-vis optical bandgap and the HOMO energy level determined previously by PES. All these data are summarized in Figure S7 and Table S2. Not surprisingly, **$(C8)_2PbI_4$** exhibits energy levels arising from the valence band (VB) and conduction band (CB) of the inorganic perovskite sublayers which is consistent with previous results obtained on 2D halide perovskites incorporating simple alkylammonium cations.[14] Regarding **$(monoNDIC8)_2PbI_4$**, its HOMO level is similar to that of **$(C8)_2PbI_4$,** indicating that the lowest energy level of **$(monoNDIC8)_2PbI_4$** also corresponds to the VB of inorganic perovskite sublayers. This result is consistent with the very deep HOMO level determined for **NDIC3**. However, the LUMO level measured for **$(monoNDIC8)_2PbI_4$** is much deeper than that of **$(C8)_2PbI_4$** and it is perfectly equal to **NDIC3** LUMO value. Therefore, we can conclude that the **$(monoNDIC8)_2PbI_4$** can form a type II heterojunction leading to a hybrid donor-acceptor structure in which the excitons can be efficiently separated into the holes and electrons located in the inorganic and organic sublayer, respectively (Figure 4).[30] Such a p-n heterojunction is fully consistent with the PL quenching of the inorganic sheets in the **$(monoNDIC8)_2PbI_4$** structure and supports the claim of an electron transfer process occurring from the CB of the inorganic perovskite monolayers to the LUMO of the NDI organic bilayers.

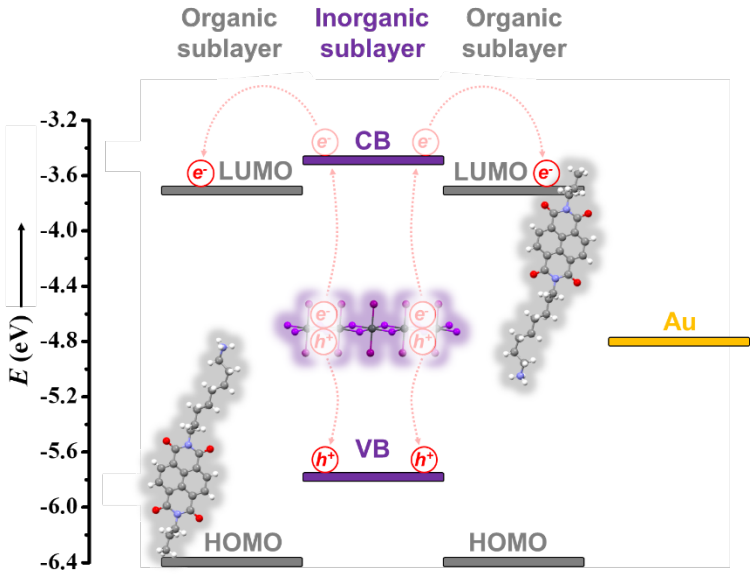

Figure 4. Relative energy levels (band alignments) of organic (gray lines) and inorganic (purple lines) sublayers for the hybrid 2D perovskite **(monoNDIC8)$_2$PbI$_4$** and schematic representation of the charge separation and electron transfer processes occurring in this type II quantum well structure (VB, valence band; CB, conduction band; HOMO, highest occupied molecular orbital; LUMO, lowest unoccupied molecular orbital). The yellow line represents the work function of gold (Au).

The type II quantum well structure of **(monoNDIC8)$_2$PbI$_4$** 2D perovskites is expected to strongly enhance charge separation and the formation of long-lived charge carriers that are promising for optoelectronic devices. We therefore, investigated the photoconduction properties of the **(monoNDIC8)$_2$PbI$_4$** perovskite with the aim of comparing them to those obtained with **(C8)$_2$PbI$_4$**. To this end, we prepared two different devices based on thin films of **(monoNDIC8)$_2$PbI$_4$** and **(C8)$_2$PbI$_4$** perovskites spin-coated onto Si/SiO_2 substrates. Planar, interdigitated gold (Au) electrodes were then deposited by thermal evaporation through a shadow mask on top of the perovskite films (Figures 6 and S8). This device configuration was chosen since **(monoNDIC8)$_2$PbI$_4$** and **(C8)$_2$PbI$_4$** perovskite thin

films show a preferential orientation of their lamellar structure parallel to the substrate (see above), leading to predominant in-plane charge transport. Note that the film thicknesses of the **(monoNDIC8)$_2$PbI$_4$** and **(C8)$_2$PbI$_4$** 2D perovskites were adjusted to 37 and 19 nm, respectively, in order to have almost the same number of inorganic perovskite sheets (*ca.* ~10) within each film.

The crystallinity and morphology of the **(monoNDIC8)$_2$PbI$_4$** and **(C8)$_2$PbI$_4$** perovskite thin films were also studied by grazing-incidence wide-angle X-ray scattering (GIWAXS) and atomic force microscope (AFM). The GIWAXS patterns are shown in Figures 5a and b and corroborate the lamellar structure expected of both films. More importantly, both patterns of **(monoNDIC8)$_2$PbI$_4$** and **(C8)$_2$PbI$_4$** confirm the ideal orientation of the lamellae, parallel to the substrates in both films as shown by the exclusive concentration of the lamellar reflections on the pattern meridian and the vertical distribution of the other (*hkl*) reflection series. The average crystallite size of **(monoNDIC8)$_2$PbI$_4$** and **(C8)$_2$PbI$_4$** in the thin film planes was also determined from the (400) spot width using the Scherrer equation with shape factor K = 0.9 and it was found to be quite similar for both films; between 7 and 10 nm.[31,32] The AFM images evidenced very homogeneous and uniform layers for both **(monoNDIC8)$_2$PbI$_4$** and **(C8)$_2$PbI$_4$** films with a root-mean-square RMS roughness of less than 5 nm, even at large probe sizes such as 20x20 μm (Figures 5a, b, S10 and S11). They also show a terrace-and-step morphology with step heights of about 38 Å and 18 Å for the **(monoNDIC8)$_2$PbI$_4$** and **(C8)$_2$PbI$_4$** thin films, respectively, consistent with the *d*-spacings obtained from XRD and GIWAXS measurements (*d* = 38.6 Å and 18.7 Å). Overall, these results demonstrate that **(monoNDIC8)$_2$PbI$_4$** and **(C8)$_2$PbI$_4$** 2D perovskite films present a comparable morphology with large crystalline domains and a similar orientation of the layered structures (parallel to the substrate), suitable for the investigation and comparison of the photoconduction properties.

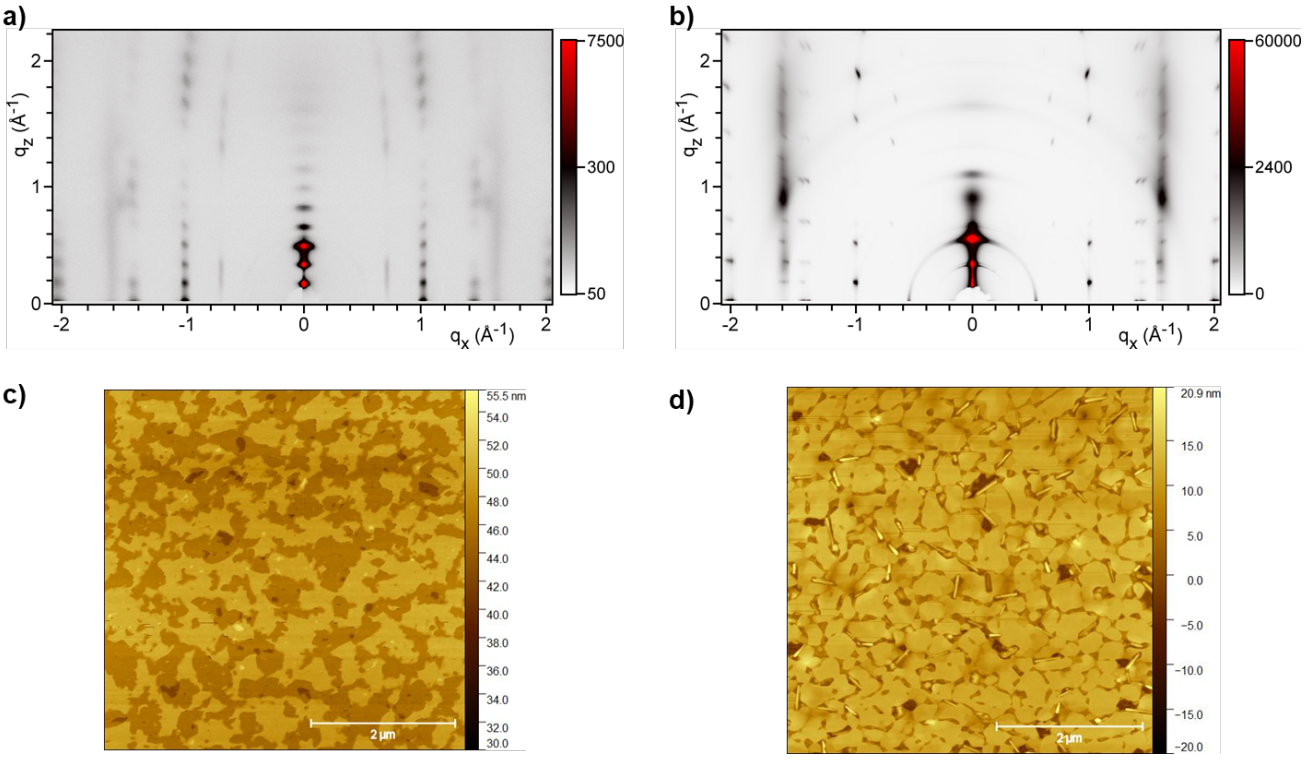

Figure 5. Grazing incidence X-ray scattering (GIWAXS) patterns of a) **(monoNDIC8)$_2$PbI$_4$** and b) **(C8)$_2$PbI$_4$** 2D perovskite thin films prepared on SiO_2/Si substrates for device fabrication. Topography AFM images of c) **(monoNDIC8)$_2$PbI$_4$** and d) **(C8)$_2$PbI$_4$** 2D perovskite thin films prepared on SiO_2/Si substrates.

The devices based on the oriented thin films of **(monoNDIC8)$_2$PbI$_4$** and **(C8)$_2$PbI$_4$** perovskites, measured at the same driving voltage of +50 V, exhibit a photocurrent upon illumination with a Xenon white-light source at a power density of *ca.* 50 mW cm^{-2} and a dark current in the range of several hundreds of fA (Figure 6b). Importantly, the **(monoNDIC8)$_2$PbI$_4$** perovskite devices showed a photocurrent above 0.6 µA, which is significantly higher than that obtained with the **(C8)$_2$PbI$_4$** devices , which are in the order of nA. Therefore, we assume that this ~40-fold enhancement observed in the **(monoNDIC8)$_2$PbI$_4$** perovskite devices (Figure 6b) originates from the separated holes and electrons generated by the charge transfer process between the organic and inorganic sublayers, occurring after the photoexcitation.

To better understand the photoconduction properties of the two perovskite structures, photocurrent-voltage dependent measurements were also carried out. The driving voltage applied between the two electrodes was gradually increased from 0 V to 100 V and the evolution of the photocurrent was recorded (Figure S12). As expected, both **$(C8)_2PbI_4$** and **$(monoNDIC8)_2PbI_4$** 2D perovskite devices showed an increase in the photocurrent with the increase of the driving voltage since a higher electric field would accelerate the drift speed of the charge carrier within the film. However, their photocurrent-voltage dependence showed two distinct characteristic behaviors. While the **$(C8)_2PbI_4$** 2D perovskite devices showed a photocurrent increase, this latter attenuates with the voltage increase (Figure S12a). On the contrary, **$(monoNDIC8)_2PbI_4$** 2D perovskite devices showed a more pronounced superlinear behavior with the voltage increase (Figure S12b). In the case of the **$(C8)_2PbI_4$** 2D perovskite, since the photogenerated charge carriers (holes and electrons) are confined within the inorganic perovskite sheets, the voltage increase would lead to the acceleration of their speeds, resulting in the enhancement of the recombination probability. However, in the case of **$(monoNDIC8)_2PbI_4$** 2D perovskite devices, the presence of NDI sublayers allows, in addition to the enhanced dissociation of the excitons (charge transfer process), the confinement of free holes and electrons in the two distinct sublayers, with the positive and negative charge carriers located on the inorganic perovskite sheets and on the organic sublayers, respectively. Consequently, the separated holes and electrons can independently migrate within their respective channels with the voltage increase, reducing the charge recombination probability. Here, we should note that the increment of the gradient in the J-V curve suggests the possibility of enhanced mobilities at higher voltages.

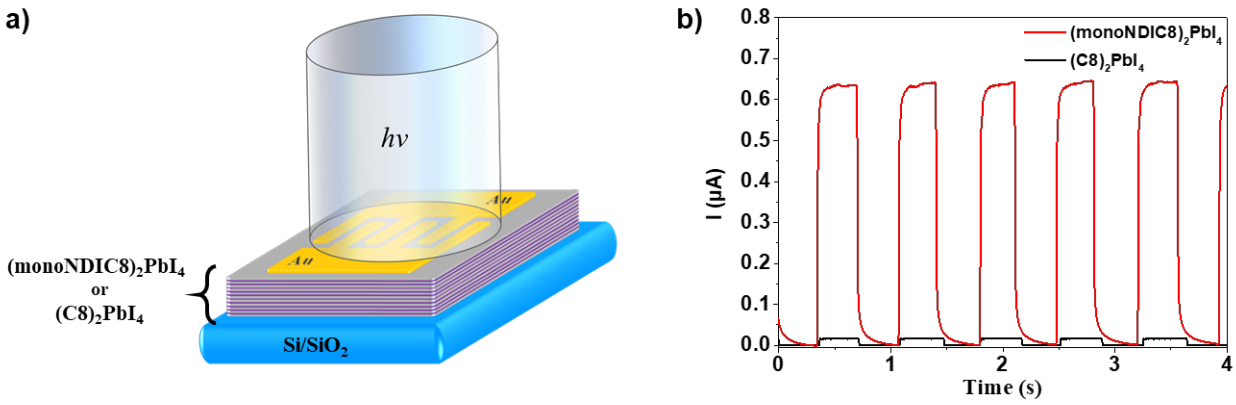

Figure 6. a) Schematic illustration of the device structure fabricated for the photoconduction property investigation of **(monoNDIC8)$_2$PbI$_4$** and **(C8)$_2$PbI$_4$** thin films. The gold (Au) interdigitated electrodes were deposited by thermal evaporation through a shadow mask with a channel length of 50 μm. b) Photocurrent of **(monoNDIC8)$_2$PbI$_4$** and **(C8)$_2$PbI$_4$** 2D perovskite devices detected between the two electrodes at a constant voltage of +50 V. The samples were illuminated by a Xenon white-light source at a power density of *ca.* 50 mW cm^{-2}.

The photoconduction properties were then studied using the irradiation of a monochromatic light. We firstly conducted photocurrent-wavelength dependent measurements to check the photoexcitation efficiency at different wavelengths (Figure S14). The photocurrent-wavelength dependent profiles of both **(C8)$_2$PbI$_4$** and **(monoNDIC8)$_2$PbI$_4$** 2D perovskite devices are almost identical to their corresponding UV-vis spectra (Figures 1b and S14). Based on these results, we decided to excite only the inorganic perovskite sublayers at the maximum of the excitonic peak wavelength. Thus, we irradiated the **(C8)$_2$PbI$_4$** and **(monoNDIC8)$_2$PbI$_4$** devices using a monochromic light at 511 and 498 nm, respectively, at a power density of ca. 4 mW cm^{-2}. Under a driving voltage of +80 V, the **(monoNDIC8)$_2$PbI$_4$** 2D perovskite devices showed photocurrent above 0.12 μA, while only ~10 nA of photocurrent was observed for the **(C8)$_2$PbI$_4$** 2D perovskite device (Figure S15). As a result, the **(monoNDIC8)$_2$PbI$_4$** perovskite device showed an enhanced photocurrent of nearly 10 times than that

of **$(C8)_2PbI_4$** ones under monochromic light. Note that this ratio is probably slightly underestimated by considering that the optical density (OD) of the **$(monoNDIC8)_2PbI_4$** layers is around 0.2 at 498 nm, while the optical density (OD) of **$(C8)_2PbI_4$** layer is about 0.3 at 511 nm, indicating less exciton formation in the **$(monoNDIC8)_2PbI_4$** layer (Figure S13). The photocurrent-voltage dependent curves of **$(C8)_2PbI_4$** and **$(monoNDIC8)_2PbI_4$** perovskite devices under monochromic light illumination were also recorded (Figure S16), and demonstrated similar behavior as those obtained under white-light illumination.

Conclusion

To summarize, we have designed a rare example of "pure" organic-inorganic 2D perovskite incorporating strong NDI acceptors between its inorganic sheets. We demonstrated that such a hybrid architecture could be easily obtained, resulting in air-stable thin films prepared *via* a solution deposition process. We evidenced that the structure consists of inorganic perovskite monolayers of metal-halide octahedra separated by bi-layers of NDI-based organic cations. The presence of strong electron-accepting moieties in this multifunctional donor-acceptor hybrid heterostructure led to a unusual type II heterojunction in which the excitons can be efficiently dissociated *via* the electron transfer process, and in which the holes and electrons can be easily confined within the inorganic and organic sublayer, respectively. Such an ultimate p-n heterojunction showed improved photoconduction properties (under white-light illumination) with a photocurrent 40 times greater than a similar 2D perovskite structure containing simply inert alkyl chains as organic components. We are convinced that such stable, layered D-A hybrid materials could be very interesting for the development of high-performance optoelectronic devices such as photodetectors or for photovoltaic conversion. This work

also supports the great potential of the organic–inorganic 2D halide perovskites which are a new class of multifunctional materials easily tunable by chemical engineering of its functional organic building blocks.

Acknowledgements

We thank Pohang Accelerator Laboratory (PAL) for giving us the opportunity to perform the GIWAXS measurements, MEST and POSTECH for supporting these experiments, Dr Hyungju Ahn for adjustments and help, and other colleagues from the 9A USAXS beamline for assistance. This work is supported by JSPS Core-to-Core Program (Grant number: JPJSCCA20180005) and by the French National Center for Scientific Research (CNRS/IRP LUX-ERIT). Mr. Z. Feng also thanks the China Scholarship Council for its support (CSC, Grant No.: 201906280233) during his research work at Kyushu University (OPERA).

References

(1) Zheng, K.; Pullerits, T. Two Dimensions Are Better for Perovskites. *J. Phys. Chem. Lett.* **2019**, *10* (19), 5881–5885. https://doi.org/10.1021/acs.jpclett.9b01568.

(2) Mao, L.; Stoumpos, C. C.; Kanatzidis, M. G. Two-Dimensional Hybrid Halide Perovskites: Principles and Promises. *J. Am. Chem. Soc.* **2019**, *141* (3), 1171–1190. https://doi.org/10.1021/jacs.8b10851.

(3) Chen, Y.; Sun, Y.; Peng, J.; Tang, J.; Zheng, K.; Liang, Z. 2D Ruddlesden-Popper Perovskites for Optoelectronics. *Adv. Mater.* **2018**, *30* (2), 1703487. https://doi.org/10.1002/adma.201703487.

(4) Paulus, F.; Tyznik, C.; Jurchescu, O. D.; Vaynzof, Y. Switched-On: Progress, Challenges, and Opportunities in Metal Halide Perovskite Transistors. *Adv. Funct. Mater.* **2021**, 2101029. https://doi.org/10.1002/adfm.202101029.

(5) Mitzi, D. B.; Feild, C. A.; Harrison, W. T. A.; Guloy, A. M. Conducting Tin Halides with a Layered Organic-Based Perovskite Structure. *Nature* **1994**, *369* (6480), 467–469. https://doi.org/10.1038/369467a0.

(6) Mousdis, G. A.; Papavassiliou, G. C.; Raptopoulou, C. P.; Terzis, A. Preparation and Characterization of [H3N(CH2)6NH3]PbI4 and Similar Compounds with a Layered Perovskite Structure. *J. Mater. Chem.* **2000**, *10* (2), 515–518. https://doi.org/10.1039/a906161d.

(7) Lemmerer, A.; Billing, D. G. Synthesis, Characterization and Phase Transitions of the Inorganic–Organic Layered Perovskite-Type Hybrids [($C_n H_{2n+1} NH_3)_2 PbI_4$], n = 7, 8, 9 and 10. *Dalton Trans* **2012**, *41* (4), 1146–1157. https://doi.org/10.1039/C0DT01805H.

(8) Perumallapelli, G. R.; Tsuda, T.; Formanek, P.; Kiriy, N.; Bakulev, V.; Simon, F.; Voit, B.; Mannsfeld, S. C. B.; Kiriy, A. New Insights into the Structure of Two-Dimensional Lead Iodide-Based Perovskites. *Org. Electron.* **2020**, *87*, 105935. https://doi.org/10.1016/j.orgel.2020.105935.

(9) Kagan, C. R.; Mitzi, D. B.; Dimitrakopoulos, C. D. Organic-Inorganic Hybrid Materials as Semiconducting Channels in Thin-Film Field-Effect Transistors. *Science* **1999**, *286* (5441), 945–947. https://doi.org/10.1126/science.286.5441.945.

(10) Matsushima, T.; Hwang, S.; Sandanayaka, A. S. D.; Qin, C.; Terakawa, S.; Fujihara, T.; Yahiro, M.; Adachi, C. Solution-Processed Organic-Inorganic Perovskite Field-Effect Transistors with High Hole Mobilities. *Adv. Mater.* **2016**, *28* (46), 10275–10281. https://doi.org/10.1002/adma.201603126.

(11) Mitzi, D. B.; Chondroudis, K.; Kagan, C. R. Design, Structure, and Optical Properties of Organic−Inorganic Perovskites Containing an Oligothiophene Chromophore. *Inorg. Chem.* **1999**, *38* (26), 6246–6256. https://doi.org/10.1021/ic991048k.

(12) Chondroudis, K.; Mitzi, D. B. Electroluminescence from an Organic−Inorganic Perovskite Incorporating a Quaterthiophene Dye within Lead Halide Perovskite Layers. *Chem. Mater.* **1999**, *11* (11), 3028–3030. https://doi.org/10.1021/cm990561t.

(13) Passarelli, J. V.; Fairfield, D. J.; Sather, N. A.; Hendricks, M. P.; Sai, H.; Stern, C. L.; Stupp, S. I. Enhanced Out-of-Plane Conductivity and Photovoltaic Performance in $n = 1$ Layered Perovskites through Organic Cation Design. *J. Am. Chem. Soc.* **2018**, *140* (23), 7313–7323. https://doi.org/10.1021/jacs.8b03659.

(14) Gao, Y.; Shi, E.; Deng, S.; Shiring, S. B.; Snaider, J. M.; Liang, C.; Yuan, B.; Song, R.; Janke, S. M.; Liebman-Peláez, A.; Yoo, P.; Zeller, M.; Boudouris, B. W.; Liao, P.; Zhu, C.; Blum, V.; Yu, Y.; Savoie, B. M.; Huang, L.; Dou, L. Molecular Engineering of Organic–Inorganic Hybrid Perovskites Quantum Wells. *Nat. Chem.* **2019**, *11* (12), 1151–1157. https://doi.org/10.1038/s41557-019-0354-2.

(15) Van Gompel, W. T. M.; Herckens, R.; Denis, P.-H.; Mertens, M.; Gélvez-Rueda, M. C.; Van Hecke, K.; Ruttens, B.; D'Haen, J.; Grozema, F. C.; Lutsen, L.; Vanderzande, D. 2D Layered Perovskite Containing Functionalised Benzothieno-Benzothiophene Molecules: Formation, Degradation, Optical Properties and Photoconductivity. *J. Mater. Chem. C* **2020**, *8* (21), 7181–7188. https://doi.org/10.1039/D0TC01053G.

(16) Wang, K.; Jin, L.; Gao, Y.; Liang, A.; Finkenauer, B. P.; Zhao, W.; Wei, Z.; Zhu, C.; Guo, T.-F.; Huang, L.; Dou, L. Lead-Free Organic–Perovskite Hybrid Quantum Wells for Highly Stable Light-Emitting Diodes. *ACS Nano* **2021**, *15* (4), 6316–6325. https://doi.org/10.1021/acsnano.1c00872.

(17) Van Gompel, W. T. M.; Herckens, R.; Van Hecke, K.; Ruttens, B.; D'Haen, J.; Lutsen, L.; Vanderzande, D. Towards 2D Layered Hybrid Perovskites with Enhanced Functionality: Introducing Charge-Transfer Complexes *via* Self-Assembly. *Chem. Commun.* **2019**, *55* (17), 2481–2484. https://doi.org/10.1039/C8CC09955C.

(18) Chondroudis, K.; Kagan, C. R. Organic–Inorganic by D. B. Mitzi. **2001**, *45* (1), 17.

(19) Saparov, B.; Mitzi, D. B. Organic–Inorganic Perovskites: Structural Versatility for Functional Materials Design. *Chem. Rev.* **2016**, *116* (7), 4558–4596.

https://doi.org/10.1021/acs.chemrev.5b00715.
(20) Gao, Y.; Wei, Z.; Hsu, S.-N.; Boudouris, B. W.; Dou, L. Two-Dimensional Halide Perovskites Featuring Semiconducting Organic Building Blocks. *Mater. Chem. Front.* **2020**, *4* (12), 3400–3418. https://doi.org/10.1039/D0QM00233J.
(21) Gélvez-Rueda, M. C.; Fridriksson, M. B.; Dubey, R. K.; Jager, W. F.; van der Stam, W.; Grozema, F. C. Overcoming the Exciton Binding Energy in Two-Dimensional Perovskite Nanoplatelets by Attachment of Conjugated Organic Chromophores. *Nat. Commun.* **2020**, *11* (1), 1901. https://doi.org/10.1038/s41467-020-15869-7.
(22) Tremblay, M.-H.; Zeidell, A. M.; Rigin, S.; Tyznik, C.; Bacsa, J.; Zhang, Y.; Al Kurdi, K.; Jurchescu, O. D.; Timofeeva, T. V.; Barlow, S.; Marder, S. R. Structural Diversity in 2,2′-[Naphthalene-1,8:4,5-Bis(Dicarboximide)- *N,N* ′-Diyl]-Bis(Ethylammonium) Iodoplumbates. *Inorg. Chem.* **2020**, *59* (12), 8070–8080. https://doi.org/10.1021/acs.inorgchem.0c00165.
(23) Proppe, A. H.; Tremblay, M.-H.; Zhang, Y.; Yang, Z.; Quintero-Bermudez, R.; Kelley, S. O.; Barlow, S.; Marder, S. R.; Sargent, E. H. Naphthalenediimide Cations Inhibit 2D Perovskite Formation and Facilitate Subpicosecond Electron Transfer. *J. Phys. Chem. C* **2020**, *124* (44), 24379–24390. https://doi.org/10.1021/acs.jpcc.0c05521.
(24) Li, X.; Yang, J.; Song, Z.; Chen, R.; Ma, L.; Li, H.; Jia, J.; Meng, J.; Li, X.; Yi, M.; Sun, X. Naphthalene Diimide Ammonium Directed Single-Crystalline Perovskites with "Atypical" Ambipolar Charge Transport Signatures in Two-Dimensional Limit. *ACS Appl. Energy Mater.* **2018**, *1* (9), 4467–4472. https://doi.org/10.1021/acsaem.8b00988.
(25) Nussbaum, S.; Socie, E.; Yao, L.; Yum, J.-H.; Moser, J.-E.; Sivula, K. Tuning Napththalenediimide Cations for Incorporation into Ruddlesden–Popper-Type Hybrid Perovskites. *Chem. Mater.* **2022**, *34* (8), 3798–3805. https://doi.org/10.1021/acs.chemmater.2c00246.
(26) Dunlap-Shohl, W. A.; Barraza, E. T.; Barrette, A.; Dovletgeldi, S.; Findik, G.; Dirkes, D. J.; Liu, C.; Jana, M. K.; Blum, V.; You, W.; Gundogdu, K.; Stiff-Roberts, A. D.; Mitzi, D. B. Tunable Internal Quantum Well Alignment in Rationally Designed Oligomer-Based Perovskite Films Deposited by Resonant Infrared Matrix-Assisted Pulsed Laser Evaporation. *Mater. Horiz.* **2019**, *6* (8), 1707–1716. https://doi.org/10.1039/C9MH00366E.
(27) Park, S. K.; Kim, J. H.; Park, S. Y. Organic 2D Optoelectronic Crystals: Charge Transport, Emerging Functions, and Their Design Perspective. *Adv. Mater.* **2018**, *30* (42), 1704759. https://doi.org/10.1002/adma.201704759.
(28) Liu, X.; Su, X.; Livache, C.; Chamoreau, L.-M.; Sanaur, S.; Sosa-Vargas, L.; Ribierre, J.-C.; Kreher, D.; Lhuillier, E.; Lacaze, E.; Mathevet, F. Investigation of Charge Transport Properties of [1]Benzothieno[3,2-b][1]-Benzothiophene Single-Crystals in Field-Effect Transistor Configuration. *Org. Electron.* **2020**, *78*, 105605. https://doi.org/10.1016/j.orgel.2019.105605.
(29) Gao, Y.; Wei, Z.; Yoo, P.; Shi, E.; Zeller, M.; Zhu, C.; Liao, P.; Dou, L. Highly Stable Lead-Free Perovskite Field-Effect Transistors Incorporating Linear π-Conjugated Organic Ligands. *J. Am. Chem. Soc.* **2019**, *141* (39), 15577–15585. https://doi.org/10.1021/jacs.9b06276.
(30) Maheshwari, S.; Savenije, T. J.; Renaud, N.; Grozema, F. C. Computational Design of Two-Dimensional Perovskites with Functional Organic Cations. *J. Phys. Chem. C* **2018**, *122* (30), 17118–17122. https://doi.org/10.1021/acs.jpcc.8b05715.
(31) Smilgies, D.-M. Scherrer Grain-Size Analysis Adapted to Grazing-Incidence Scattering with Area Detectors. Erratum. *J. Appl. Crystallogr.* **2013**, *46* (1), 286–286.

https://doi.org/10.1107/S0021889812050054.
(32) Ribierre, J.-C.; Li, Z.; Liu, X.; Lacaze, E.; Heinrich, B.; Méry, S.; Sleczkowski, P.; Xiao, Y.; Lafolet, F.; Hashizume, D.; Aoyama, T.; Uchiyama, M.; Wu, J. W.; Zaborova, E.; Fages, F.; D'Aléo, A.; Mathevet, F.; Adachi, C. A Solvent-Free and Vacuum-Free Melt-Processing Method to Fabricate Organic Semiconducting Layers with Large Crystal Size for Organic Electronic Applications. *J. Mater. Chem. C* **2019**, *7* (11), 3190–3198. https://doi.org/10.1039/C8TC04834G.

Table of Contents

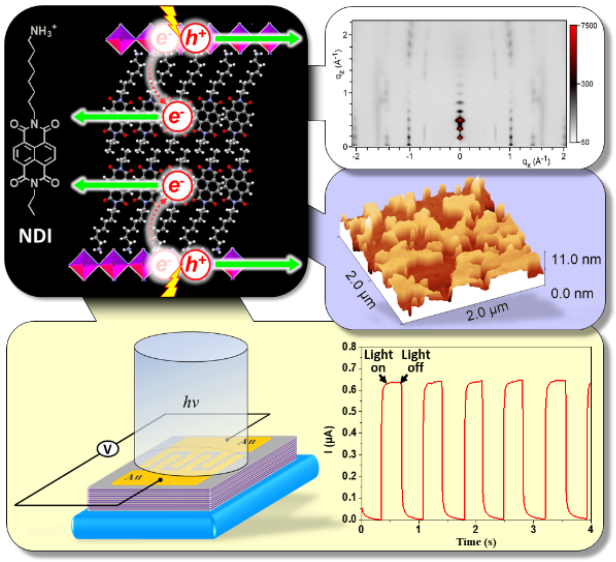

An organic-inorganic 2D perovskite incorporating strong acceptor naphthalene diimide (NDI) building blocks between inorganic sheets was prepared, leading to a multifunctional donor-acceptor hybrid type II heterostructure. In such an ultimate p-n heterojunction, excitons can be efficiently dissociated *via* electron transfer process and holes and electrons can be easily confined in the inorganic and organic sublayer, respectively, producing improved photoconduction properties.